Tethered membranes far from equilibrium: Buckling dynamics

Dorel Moldovan[1] and Leonardo Golubovic[2,*]
[1]*Materials Science Division, Argonne National Laboratory, Argonne, Illinois 60439*
[2]*Department of Physics, Harvard University, Cambridge, Massachusetts 02138*
(Received 21 April 1999)

We study the dynamics of the classical Euler buckling of compressed solid membranes. We relate the membrane buckling dynamics to phase ordering phenomena. Membranes develop a wavelike pattern whose wavelength grows, via coarsening, as a power of time. We find that evolving membranes are similar to growing surfaces (''growing interfaces'') whose transverse width grows as a power of time. The morphology of the evolving membranes is characterized by the presence of a network of growing ridges where the elastic energy is mostly localized. We used this fact to develop a scaling theory of the buckling dynamics that gives analytic estimates of the coarsening exponents. Our findings show that the membrane buckling dynamics is characterized by a distinct scaling behavior not found in other coarsening phenomena. [S1063-651X(99)04510-9]

PACS number(s): 05.70.Ln, 82.20.Mj, 46.32.+x, 05.40.−a

I. INTRODUCTION

Polymerized, tethered membranes, generalizing flexible polymers, have attracted much interest in recent years. Their *thermal equilibrium* properties have been studied recently numerically [1–5], experimentally [6,7], and analytically [8–10]. In a recent Letter [11] we addressed the problem of far-from-equilibrium buckling dynamics of tethered membranes. The present work is devoted to the study of the buckling dynamics of tethered membranes outlined before briefly in Ref. [11]. Here we address the question of the *far-from-equilibrium* buckling dynamics of such membranes (thin elastic sheets), moving in a viscous medium. Mechanical instabilities of elastic manifolds pose a rich spectrum of problems that are still largely unresolved despite great effort. Classical examples are buckling instabilities of thin sheets [12], which are of great importance in safety design and development of energy absorbing structures [13]. There are large varieties of phenomena involving deformations of thin elastic sheets (membranes). These, potentially, span a wide range of scales, from phospholipid membranes [14] and thin sheets of graphite oxide in aqueous suspensions [7] to the raglike structures found in molybdenum disulphite [15] and spectrin skeleton of red blood cell membranes [16]. A good example is the buckling instability of polymerized monolayers of insoluble amphiphiles adsorbed at the air-water interface, studied by Bordieu *et al.*, and more recently by Saint-Jalmes and Gallet [17]. Buckling of a membrane can be induced in a variety of ways, for example, simply by applying a compressional lateral strain. Another related class of phenomena is the buckling due to internal strains, which plays an important role in heteroepitaxial growth, such as, for example, the growth of SiGe multilayers on Si substrates [18].

In practice, strains causing buckling are frequently of thermal origin [18]. Membranes immersed in fluids may buckle if the temperature of the fluid is raised and the boundary of the membrane is held fixed. The temperature jump would expand a membrane with a free boundary. It thus effectively induces a *uniform* compressive strain ϵ in the membrane with a fixed boundary. If $\varepsilon > \varepsilon_c \sim L^{-2}$, such a thermally strained membrane will buckle; L is the linear dimension of the membrane.

Historically, Euler's buckling instability is the very first example for bifurcation phenomena and the paradigm for subsequent theories of phase transitions [12]. Still, the dynamics of this phenomenon has been addressed in depth only recently, for the case of tethered membranes [11], and flexible chains of molecules [19]. In itself, buckling involves a spontaneous symmetry breaking. Thus, a compressed membrane may buckle either up or down (breaking of Z_2, Ising-type symmetry). Therefore, buckling is a practically interesting analog of the phase ordering phenomena. In this paper, we address extensively the fundamentals of buckling dynamics, that is, we study *how* initially compressed membranes reach the final buckled configuration at long times. We elucidate deep relationships of the membrane buckling dynamics to phase ordering processes [20–22], such as the mound growth recently observed in molecular beam epitaxy [23–25]. We find that membrane buckling dynamics can be envisioned as a phase ordering process in which membrane slope plays the role of the order parameter. We show that membrane buckling dynamics forms a distinct class of the phase ordering processes characterized by a scaling behavior not found before in other coarsening phenomena [20–25]. Membrane transverse displacements develop a wavelike pattern in two dimensions with a wavelength that grows, via a coarsening process, as a power of time. Evolving membranes are like growing surfaces (''growing interfaces'') whose transverse width grows as a power of time. The morphology of evolving membranes is characterized by the presence of a network of growing ridges where the elastic energy is mostly concentrated. We used this fact to develop a scaling theory of the buckling dynamics that gives analytic estimates of the coarsening exponents.

The balance of our paper is as follows. We discuss the model for the tethered membrane in Sec. II. In Sec. III, our molecular-dynamics (MD) simulations results for the mem-

*Permanent address: Physics Department, West Virginia University, Morgantown, WV 26506.

brane buckling dynamics are presented. A scaling theory of the buckling dynamics based on the evidence of the existence of high energy concentration regions, ''ridges,'' across the surface of the membrane is proposed in Sec. IV. We conclude in Sec. V where we summarize our findings and possible future directions of investigation. In the Appendix, we generalize the scaling analysis of Sec. IV to discuss the effects of long range viscous forces on membrane buckling dynamics (so-called Zimm dynamics).

II. THE MODEL

A tethered membrane is a system of particles connected to form a triangular two-dimensional (2D) mesh embedded in three dimensions. Each particle is labeled by an internal discrete coordinate $x=(x_1,x_2)$ denoting its position on the mesh. Its actual position in the 3D space is given by the three-dimensional vector $\vec{r}(x_1,x_2)$. The particles are arranged in a triangular array, interacting with their nearest neighbors by a simple Gaussian spring potential. The membrane's bending energy is modeled by a ferromagneticlike interaction between the normals to the nearest-neighbor ''plaquettes'' [10]. Thus, the net elastic potential energy of the membrane reads

$$U=\sum_{\langle xx'\rangle}\tfrac{1}{2}(|\vec{r}_x-\vec{r}_{x'}|-r_0)^2+\kappa\sum_{\langle\alpha\beta\rangle}(1-\vec{n}_\alpha\cdot\vec{n}_\beta), \quad (1)$$

where x and x' label the nodes and $r_0=1.0$ is the equilibrium bond (''spring'') length (as usual, $\langle xx'\rangle$ signifies the bond between nearest neighbors x and x'). The subscripts α and β label the neighboring faces (triangles) of the surface, $\vec{n}_\alpha$ is the unit normal vector to the face α, κ is the bending rigidity, and $\langle\alpha\beta\rangle$ signifies the nearest-neighbor plaquettes.

We have studied membranes that are hexagonal in shape of linear dimensions up to $L=500$ (L is the number of particles on the largest diagonal), that contain up to 186 751 particles (see Fig. 1). To minimize the finite size effects, we have done all the calculations (spatial averages) of physical quantities on a subset of the large membrane. The subset we used to calculate the spatial averages was a hexagonal region of size $L_{sm}=250$ (a subset with $N=45\,019$ particles) centered in the middle of the large membrane.

III. MOLECULAR-DYNAMICS SIMULATIONS OF MEMBRANE BUCKLING DYNAMICS

Here we report the results of large-scale molecular-dynamics simulations of tethered membranes, initially in a precompressed state (see Fig. 1). The dynamical model studied here by MD is the standard overdamped Rouse dynamics,

$$\gamma\frac{d\vec{r}_x}{dt}=-\frac{\partial U}{\partial\vec{r}_x}+\vec{\eta}_x(t), \quad (2)$$

of the tethered membrane. Here $\vec{r}_x(t)$ is the position of the particle at time t, γ is the viscous friction coefficient, and $\vec{\eta}_x(t)$ is thermal noise. The membrane is initially in a flat configuration with all its bonds compressed by ε (e.g., $\varepsilon=0.1$ for the simulations discussed here) and with fixed boundary (''frame'') of hexagonal shape (see Fig. 1). Naturally, the frame linear size is 10% smaller than that of a fully relaxed membrane (with zero elastic energy). We focus here on the membrane dynamics without thermal noise (''zero-temperature'' dynamics), i.e., we set $\vec{\eta}_x(t)=0$ in Eq. (2). The only randomness used here was small initial random transverse displacements around initially compressed and, therefore, unstable flat configurations of the membrane (just to enable the membrane to start moving).

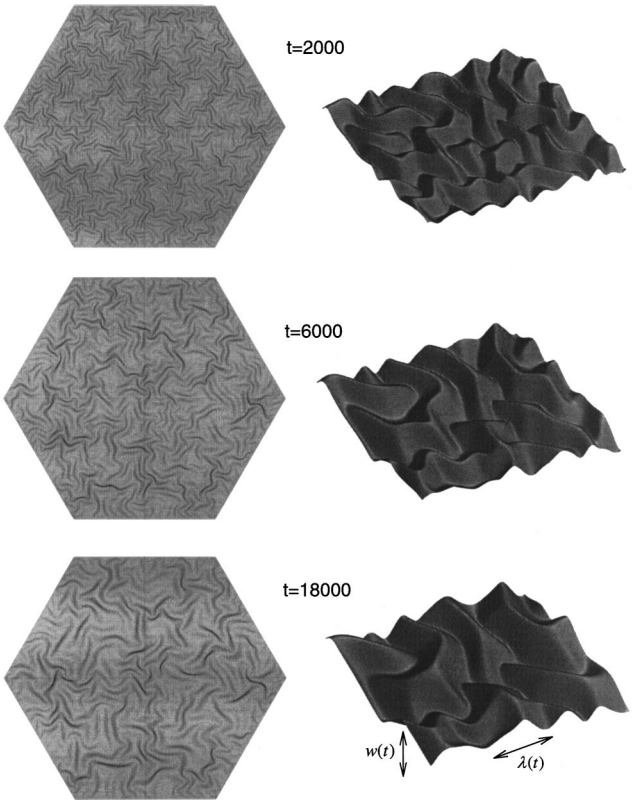

FIG. 1. Snapshot of the evolving membrane at times $t=2000$, 6000, and 18 000. The membrane is initially in the x-y plane. The membrane configurations are being viewed from two perspectives: along the z axis, the left column that depicts the whole membrane, and along a direction making an angle with the z axis in order to magnify a 6% selection taken from the midsection of the whole membrane (the right column). The left column perspective makes visible only molecular displacements parallel to the x-y plane.

Figure 1 shows snapshots of configurations that display the time evolution of the $N=186\,751$ particle membrane at times $t=2000$, 6000, and 18 000. Each configuration is being viewed from two perspectives; along the z axis for the whole membrane (the left-hand column), and along a direction making an angle with the z axis, to magnify a smaller membrane portion (the right-hand column). The membrane is initially in the x-y plane. As can be seen from Fig. 1, buckling instability, due to negative internal strains, amplifies transverse displacements and produces a chaotic dynamics. Manifestly, membrane transverse displacements $r_T(x,t)$, along the z axis, develop an evolving wavelike pattern of *mounds* characterized by a growing lateral length scale $\lambda(t)$ (''wavelength''). Notably, membrane morphology is characterized by the presence of a network of highly curved regions, *ridges* that bound more flat regions, mound *facets* with linear size $\sim\lambda(t)$. Associated with the growth of the mound lateral size $\lambda(t)$ is a growth of the membrane's transverse spread $w(t)$

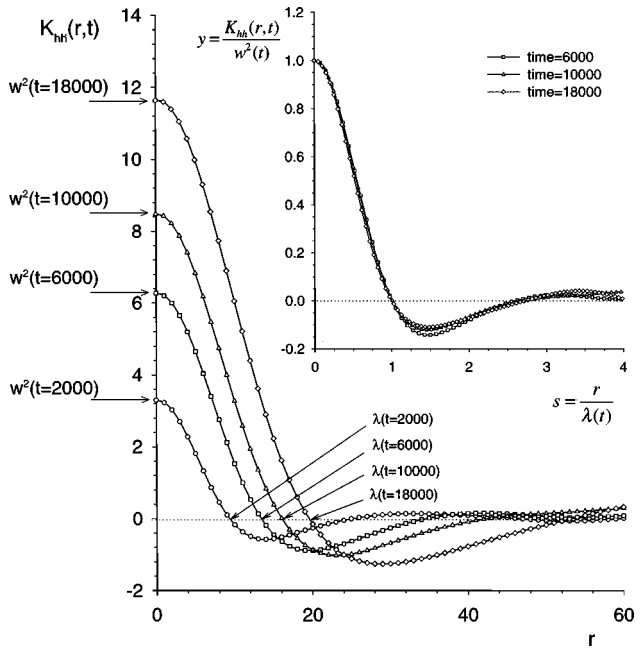

FIG. 2. The height-height correlation functions $K_{hh}(r,t)$ versus r for four values of the time $t=2000$, 6000, 10 000, and 18 000. The inset shows the collapse of the correlation functions into a single curve $y=\psi(x)$. Here $y=K_{hh}(r,t)/K_{hh}(r=0,t)$ and $x=r/\lambda(t)$, where $\lambda(t)$ is the first zero of $K_{hh}(r,t)$.

(''width'') along the z axis (see Fig. 1). $w(t)$ can be thought of as the typical height of a mound. We quantify it as $[w(t)]^2=\langle[r_T(x,t)-\langle r_T\rangle]^2\rangle$. Here and in the following, $\langle\,\rangle$ stands for spatial average, defined for any quantity $A(x,t)$ as $\langle A(x,t)\rangle=\Sigma_x A(x,t)/N$.

In order to quantitatively characterize the surface morphology, we have calculated, apart from the membrane width $w(t)$, the height-height correlation function:

$$K_{hh}(r,t)=\langle r_T'(x,t)r_T'(x+r,t)\rangle, \tag{3}$$

where $r_T'(x,t)=r_T(x,t)-\langle r_T\rangle$ is the relative transverse displacement with respect to the average height of the membrane (in these simulations $\langle r_T\rangle\approx 0$ at all times). This correlation function (see Fig. 2) has an oscillatory character reflecting wavelike membrane patterns in Fig. 1. We used the height-height correlation function to find the membrane wavelength (mound lateral size) $\lambda(t)$, by identifying it with the position of the first zero crossing of $K_{hh}(r,t)$, see Fig. 2 [19–25]. We thus find that the membrane transverse width $w(t)$ and wavelength $\lambda(t)$ both grow as powers of time,

$$w(t)\sim t^{\beta}, \quad \lambda(t)\sim t^{n_c}, \tag{4}$$

with the exponents $\beta=0.29\pm 0.01$ and $n_c=0.28\pm 0.01$. This is documented in Figs. 3 and 4, which show the width and wavelength as functions of time, on both linear and logarithmic scales. Moreover, as documented in the inset to Fig. 2, height-height correlation functions obtained at different times collapse into a single scaling function $y=\psi(s)$; here $y=K_{hh}(r,t)/K_{hh}(r=0,t)=K_{hh}(r,t)/w^2$, and $s=r/\lambda(t)$. Thus, at long times,

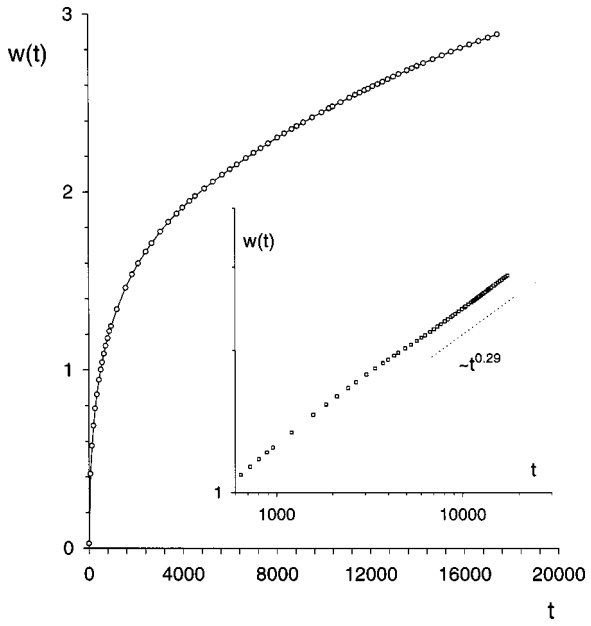

FIG. 3. The membrane transverse width $w(t)$ versus time. $w(t)$ measures the height of the mounds comprising the membrane profile. The log-log plot gives the scaling $w(t)\sim t^{0.29}$.

$$K_{hh}(r,t)=w^2(t)\psi\left(\frac{r}{\lambda(t)}\right), \tag{5}$$

where $\psi(s)$ is a scaling function satisfying $\psi(0)=1$ and $\psi(1)=0$.

As w and λ correspond, respectively, to the typical mound height and mound lateral size, the ratio w/λ corresponds to the average mound slope. Due to the fact that the two exponents β and n_c are essentially equal, we see that the average

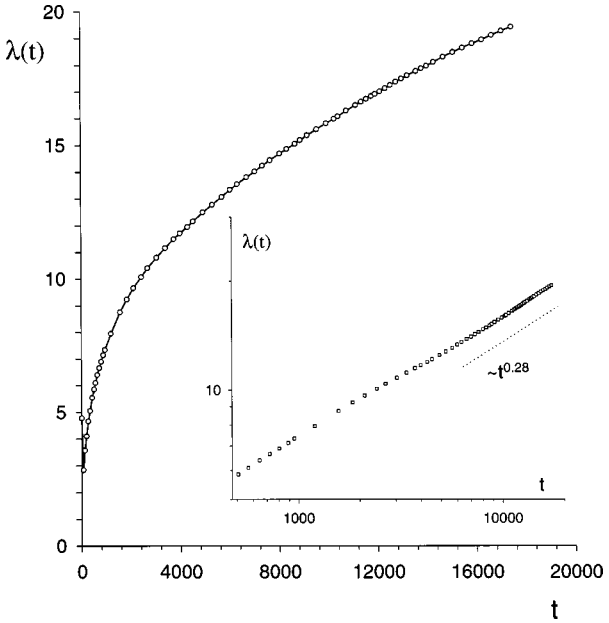

FIG. 4. The time evolution of the first zero of the height-height correlation function $K_{hh}(r,t)$, called $\lambda(t)$, the ''wavelength'' of the membrane wavelike pattern. $\lambda(t)$ measures the lateral size of the mounds comprising the membrane profile. The log-log plot gives the scaling $\lambda(t)\sim t^{0.28}$.

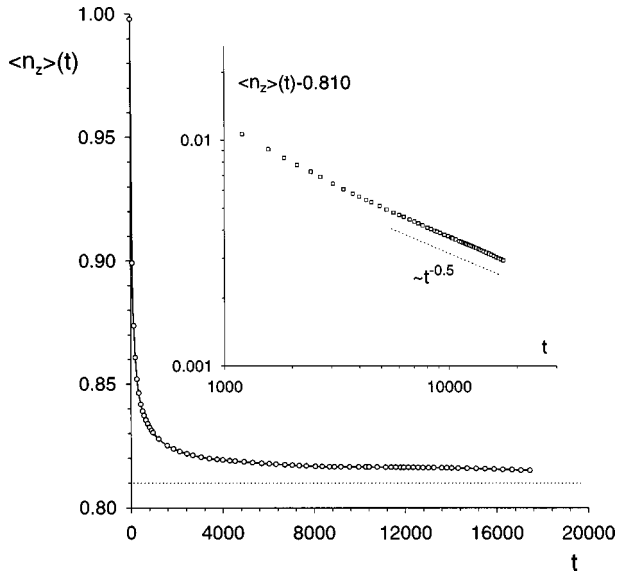

FIG. 5. The time relaxation of the average z component of the normal unit vector to the surface of the membrane $\langle n_z \rangle$. The log-log plot gives the scaling $[\langle n_z \rangle(t) - \langle n_z \rangle(t=\infty)] \sim t^{-0.50}$ [where $\langle n_z \rangle(t=\infty) = 0.810$].

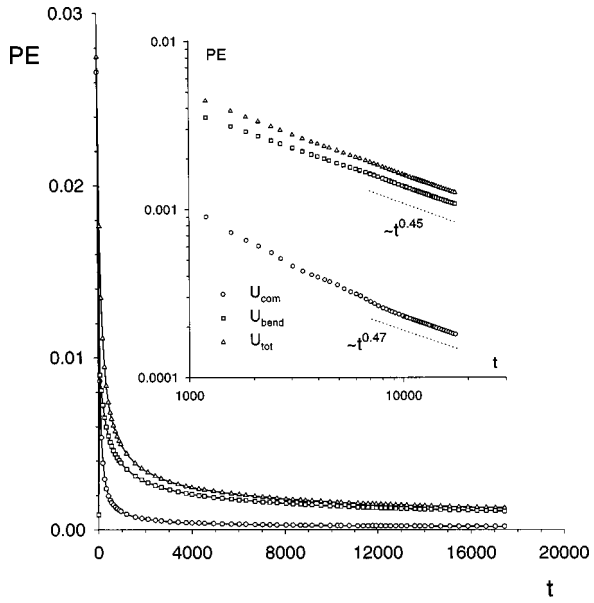

FIG. 6. The time evolution of membrane elastic potential energies (PE): total potential energy $U = U_{\text{bend}} + U_{\text{com}}$, bending energy U_{bend}, and compressional energy U_{com}, per particle versus time.

slope of the mounds stabilizes to a constant value at long times. To rationalize this, consider the average value of the z component of the unit normal vector to the surface, $\langle n_z \rangle$. From simple geometrical considerations, we have the following estimate:

$$\langle n_z \rangle = \frac{A_{\Delta 0}}{A_\Delta} = \frac{r_0^2 (1-\varepsilon)^2}{l^2(t)} \xrightarrow[t \to \infty]{} \frac{r_0^2 (1-\varepsilon)^2}{r_0^2} = (1-\varepsilon)^2, \tag{6}$$

where $A_{\Delta 0}$ is the area of an equilateral triangle plaquette in the initial ($t=0$) horizontal position with all the bonds precompressed by ε, whereas A_Δ is the area of the same plaquette tilted at time t when the bond length is $l(t)$. At long times, $l(t)$ approaches r_0 (the relaxed bond length) and the mound slope $w(t)/\lambda(t) \approx \sqrt{1 - \langle n_z \rangle^2}/\langle n_z \rangle$ stabilizes to a value determined by the externally imposed strain ε. Equation (6) yields

$$\frac{w(t)}{\lambda(t)} \sim \sqrt{\varepsilon} \tag{7}$$

for $\varepsilon \ll 1$. Figure 5 from our simulations shows the time evolution of $\langle n_z \rangle$. We can see that indeed it stabilizes at long times at the value $\langle n_z \rangle(t=\infty) \cong 0.810$. In fact, this value is in perfect agreement with Eq. (6), with $\varepsilon = 0.1$, as used in our simulations. From our simulations we find $[\langle n_z \rangle(t) - \langle n_z \rangle(t=\infty)] \sim t^{\zeta}$ with $\zeta = -0.50 \pm 0.01$ (see Fig. 5).

We obtain additional insight into the membrane scaling behavior by considering the decay of the elastic potential energy, see Fig. 6. The net elastic energy U is the sum of the compressional energy U_{com} [the first term on the right-hand side of Eq. (1)] and the bending energy U_{bend} [the second term on the right-hand side of Eq. (1)]. We see that at long times,

$$U_{\text{com}}(t) \sim \frac{1}{t^{\delta'}}, \tag{8}$$

with $\delta' = 0.47 \pm 0.01$, whereas

$$U_{\text{bend}}(t) \sim \frac{1}{t^{\delta''}}, \tag{9}$$

with $\delta'' = 0.45 \pm 0.01$, see Fig. 6. Numerically, the scaling exponents δ' and δ'' are nearly equal. We note that the ratio $U_{\text{bend}}/U_{\text{com}}$ is about 5 at the longest time of the simulation. The total elastic potential energy $U(t) = U_{\text{bend}}(t) + U_{\text{com}}(t)$ decays with an exponent close to $\delta'' \approx \delta'$. This is documented in Fig. 6, where we find

$$U(t) \sim \frac{1}{t^{\delta}}, \tag{10}$$

with $\delta = 0.46 \pm 0.01$.

IV. SCALING THEORY OF MEMBRANE BUCKLING DYNAMICS

In this section we propose a scaling theory of membrane buckling dynamics. It is similar in spirit to Bray's recent scaling theory of coarsening processes such as spinodal decomposition [20–22]. This approach relates the dynamics of the coarsening processes in dissipative systems to the rate of extinction of energy rich regions, such as domain walls in Ising ferromagnets. Such energy rich configurations, similar to domain walls, are present also in our case, in the form of elliptically shaped ridges of length $\lambda(t)$ which bound more flat regions, facets with area $\approx \lambda^2(t)$, as noted in Sec. III. This is further documented in Fig. 7 from our simulations, which depicts bending energy density distribution over the surface of the membrane at time $t = 6000$ for a small portion (50×50) of the membrane. Notably, the elastic energy is

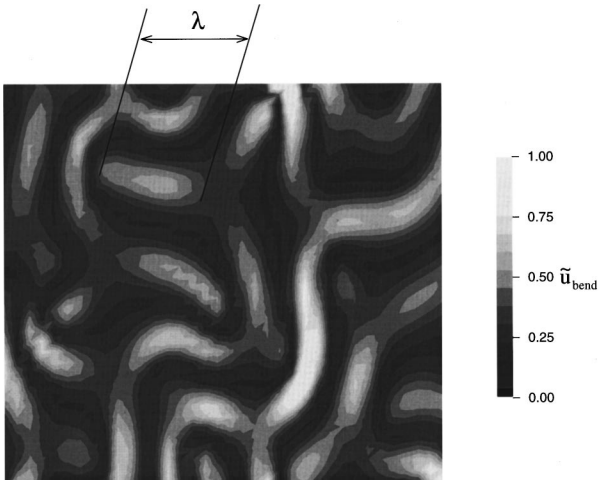

FIG. 7. The elastic bending energy density for a small portion of the membrane (50×50) at time $t=6000$. Here, $\tilde{u}_{\rm bend}(x)=u_{\rm bend}(x)/(u_{\rm bend})_{\rm max}$, where $(u_{\rm bend})_{\rm max}$ is the maximum value of the local bending energy density, i.e., bending energy per particle $u_{\rm bend}(x)$. Notably, the elastic energy is localized in elliptically shaped ridges (bright regions), whereas larger dark areas are nearly flat facets characterized by low elastic energy density.

localized into a relatively small portion of the membrane area occupied by a network of elliptically shaped ridges of length $\lambda(t)$ (see Fig. 7). A ''unit cell'' of this random network has the area $\approx\lambda^2(t)$ coinciding with the typical area of a facet.

As there is of the order one ridge per area $\approx\lambda^2(t)$, the average elastic energy per particle, i.e., energy per unit area, is

$$u=\frac{U_{\rm ridge}(\lambda)}{\lambda^2}, \tag{11}$$

where $U_{\rm ridge}(\lambda)$ is the energy of a single ridge of length λ. For ridges of deformed membranes, it has been recently suggested that

$$U_{\rm ridge}(\lambda)\sim\lambda^{\nu}, \tag{12}$$

with $\nu=\frac{1}{3}$ [26,27]. Thus, by Eq. (11),

$$u\sim\frac{1}{\lambda^{2-\nu}}. \tag{13}$$

So, the decay of the elastic energy density from simulations in Fig. 7, with $u\sim t^{-\delta}$, is related to the growth of $\lambda(t)$ by Eq. (13). As $u\sim t^{-\delta}$, we find, by Eq. (13),

$$\lambda\sim t^{n_c}, \tag{14}$$

with

$$n_c=\frac{\delta}{2-\nu}. \tag{15}$$

To proceed further, we use the energy dissipation relation

$$\frac{1}{\gamma}\frac{dU}{dt}=-\sum_{x=1}^{N}\left\langle\left(\frac{\partial\vec{r}_x}{\partial t}\right)^2\right\rangle, \tag{16}$$

implied by the equation of motion (2). In terms of the energy per particle $u=U/N$, Eq. (16) reads

$$\frac{1}{\gamma}\frac{du}{dt}=-\left\langle\left(\frac{\partial\vec{r}}{\partial t}\right)^2\right\rangle. \tag{17}$$

By using Eq. (17) with $u\sim t^{-\delta}$, and $\partial r/\partial t\sim w/t\sim t^{\beta-1}$, we obtain the scaling relation $t^{-\delta-1}\sim t^{2(\beta-1)}$, i.e.,

$$\delta+1=2(1-\beta). \tag{18}$$

Finally, as the mound slope $w(t)/\lambda(t)$ saturates to a constant value at long times t, one has $w(t)\sim\lambda(t)$, i.e., $t^{\beta}\sim t^{n_c}$, and, thus,

$$\beta=n_c. \tag{19}$$

Equations (15), (18), and (19) form the basic set of scaling relations in our analysis. By using them, we can express the scaling indices β, n_c, and δ in terms of a single scaling index ν. By combining Eqs. (15), (18), and (19), we thus find

$$\delta=\frac{2-\nu}{4-\nu}\quad\text{(Rouse dynamics)} \tag{20}$$

and

$$\beta=n_c=\frac{1}{4-\nu}\quad\text{(Rouse dynamics)}. \tag{21}$$

Equations (20) and (21) are the fundamental results of our scaling analysis. With $\nu=\frac{1}{3}$, as suggested in [26,27], our equations (20) and (21) yield

$$\delta=\tfrac{5}{11}\cong0.45,\quad\beta=n_c=\tfrac{3}{11}\cong0.27\quad\text{(Rouse dynamics)} \tag{22}$$

in good agreement with our simulation results of Sec. III.

Rouse dynamics does not incorporate the long range effects of hydrodynamic backflows of fluid media on moving membranes, so-called Zimm effects [28]. These effects can be readily included into our scaling analysis. We find for the Zimm dynamics,

$$\delta=\frac{2-\nu}{3-\nu}\quad\text{(Zimm dynamics)} \tag{23}$$

and

$$\beta=n_c=\frac{1}{3-\nu}\quad\text{(Zimm dynamics)}. \tag{24}$$

The derivation of Eqs. (23) and (24) is presented in the Appendix. With $\nu=\frac{1}{3}$ [26], we thus have

$$\delta=\tfrac{5}{8},\quad\beta=n_c=\tfrac{3}{8}\quad\text{(Zimm dynamics)}. \tag{25}$$

Overall, the analysis of this section shows that basic features of the buckling dynamics can be understood by invoking energetics of ridges and applying a scaling approach similar to that used to describe the phase ordering in magnetic systems [22]. Our analysis shows that the buckling dynamics constitutes a new class of coarsening phenomena ex-

hibiting novel scaling behavior characterized by exponents [such as those in Eqs. (22) and (25)] not found before in magnetic systems or elsewhere [20–25].

V. CONCLUSIONS

In summary, here we have studied the fundamentals of the membrane buckling dynamics, that is, how an initially flat membrane under external strain imposed by fixed boundaries reaches the equilibrium buckled configuration at long times. We find that evolving membranes develop growing wavelike patterns. We have revealed here that the dynamics of buckling is similar in nature to phase ordering processes such as spinodal decomposition. Membrane buckling dynamics is analogous to phase ordering processes such as the growth of ordered domains in magnetic systems below the critical temperature. Membranes develop nearly flat growing domains (facets) whose slope plays a role similar to that of an order parameter in phase ordering processes. Membranes evolve via a stochastic coarsening process that has associated with it power law growth of length scales that characterize the evolving membrane. We find that the coarsening exponents for the transverse membrane width $w(t) \sim t^{\beta}$ and for the length scale of the facets $\lambda(t) \sim t^{n_c}$ are nearly equal. Such a growth of $w(t)$, with $\beta \cong n_c$, is strikingly similar to the interfacial coarsening process recently found to occur in molecular beam epitaxy (so-called pyramidal or mound growth [23–25]). The morphology of the evolving membranes is characterized by the presence of a network of growing ridges where the elastic energy is mostly localized. We used this fact to develop a scaling theory of the buckling dynamics that gives analytic estimates of the coarsening exponents. These estimates are in good agreement with our simulation results. Finally, our results show that the membrane buckling dynamics constitutes a new class of coarsening phenomena characterized by novel scaling behaviors, such as those in Eqs. (22) and (25), not found in magnetic systems or elsewhere [20–25].

We end by stressing some features of the present study and anticipating directions for future studies. First of all, we emphasize that the stochastic nature of the membrane buckling dynamics discussed in this work is not due to thermal noise, which was, in fact, switched off in the simulations presented here. In fact, interestingly, the stochasticity is produced dynamically by the nonlinear nature of the system and by the presence of many degrees of freedom. Similar dynamical stochasticity occurs in phase ordering processes, e.g., in spinodal decomposition in time-dependent Ginzburg-Landau models [22]. Moreover, in these systems, thermal noise was found to be typically irrelevant for the coarsening process, i.e., the presence of a white noise does not affect coarsening exponents, such as n_c. It would be interesting to investigate if this remains true in the membrane case also (especially in view of the anomalous membrane elasticity revealed by Nelson and Peliti [9]). Another extension of the present study would be to investigate buckling dynamics of membranes adsorbed at fluid interfaces. These systems are generalizations of those discussed here. For adsorbed membranes, in addition to Zimm effects (Sec. IV and Appendix), one must include membrane spontaneous curvature as well as hydrostatic forces that yield a saturation of the membrane wavelength $\lambda(t)$ at long times. Such a study of adsorbed membranes would be relevant for understanding dynamical aspects of the buckling of polymerized surfactant monolayers adsorbed at fluid interfaces, investigated in recent experiments [17]. Other possible extensions of the present work could be to study the dynamics of buckling with no *external* friction mechanism present. Indeed, though many applications deal with membranes embedded in fluid media, it would also be interesting to study buckling dynamics in the absence of any external friction, e.g., the Hamiltonian buckling dynamics of the membrane, or phenomenological models incorporating *internal* friction mechanisms [30], which may be more relevant for the buckling of thin sheets in air.

Finally, various other modes of applying the buckling strain may be investigated. Our present study dealt with membranes evolving under a constant external strain imposed by keeping the boundaries of the membrane fixed (fixed frame). The membrane is thus initially under a uniform compressive strain that relaxes during the subsequent buckling dynamics. A natural extension of the present study is to investigate the case with initially relaxed membranes under an external strain which is gradually increased (i.e., the frame size is decreased) to the final value. The resulting membrane behavior will certainly depend on how the external strain is increased and extensive future studies should address many different possible ways of loading the buckling strain.

ACKNOWLEDGMENTS

We thank Andrew Karwowski, Arnoud Saint-Jalmes, Charles Knobler, and James P. Sethna for discussions. This work was supported by Mylan Laboratories, Inc. and by NSF/WV EPSCoR. The simulations were performed on the CM-5 parallel computer at West Virginia University.

APPENDIX

In this appendix we generalize the scaling analysis of Sec. IV to discuss the effects of long range viscous forces on the membrane buckling dynamics. For this purpose we consider a more general membrane dynamics of the form

$$m \frac{\partial^2 \vec{r}(x,t)}{\partial t^2} = -\sum_{x'} \gamma(x-x') \frac{\partial \vec{r}(x',t)}{\partial t} - \frac{\partial U}{\partial \vec{r}(x,t)}. \tag{A1}$$

Here m is the mass of a membrane molecule, whereas the first term on the right-hand side of Eq. (A1) is a nonlocal viscous force. For $m=0$ and $\gamma(x-x') = \gamma \delta_{x,x'}$, Eq. (A1) reduces to the standard Rouse dynamics disccussed in previous sections. Here we discuss the effects of a long ranged viscous kernel $\gamma(x-x')$, decaying as a power law for large $|x-x'|$. By multiplying Eq. (A1) by $\partial \vec{r}(x,t)/\partial t = v(x,t)$ and summing over x, one obtains the energy dissipation equation

$$\frac{d}{dt}[K+U] = -P_{\mathrm{diss}}, \tag{A2}$$

where $K=\Sigma(m/2)v^2(x,t)$ is the total kinetic energy of the membrane, U is the elastic potential energy of the membrane given by Eq. (1), and $P_{\rm diss}$ is the power dissipated by the viscous friction,

$$P_{\rm diss}=+\sum_x \sum_{x'} \gamma(x-x')v(x,t)v(x',t). \tag{A3}$$

By Eqs. (A2) and (A3), for a large membrane of N molecules, one has

$$\frac{d}{dt}[k+u]=-p_{\rm diss}, \tag{A4}$$

where $k=K/N=(m/2)\langle v^2(x,t)\rangle$ and $u=U/N$ are, respectively, kinetic and potential energy per membrane molecule, whereas $p_{\rm diss}$ signifies the viscous friction power per molecule,

$$p_{\rm diss}=\frac{P_{\rm diss}}{N}=\sum_r \gamma(r)K_{vv}(r). \tag{A5}$$

Here

$$K_{vv}(r)=\langle v(x+r)v(x)\rangle \tag{A6}$$

is the velocity correlation function. $p_{\rm diss}$ in Eq. (A5) can be represented as

$$p_{\rm diss}=\int \frac{d^2q}{(2\pi)^2}\tilde{K}_{vv}(q)\tilde{\gamma}(q), \tag{A7}$$

where we introduce the Fourier transform, defined in the usual way (i.e., for any quantity $A(x)$ we have $\tilde{A}(q)=\Sigma_x A(x)e^{-iqx}$, $A(x)=(1/N)\Sigma_q\tilde{A}(q)e^{iqx}=\int[d^2q/(2\pi)^2]\tilde{A}(q)e^{iqx}$). In the spirit of Eq. (5) of Sec. III, we consider the velocity correlation function of the form

$$K_{vv}(r)=K_{vv}(0)f\left(\frac{r}{\lambda}\right), \tag{A8}$$

$f(s)$ is a scaling function [$f(0)=1$]. Here $K_{vv}(0)=\langle v^2\rangle=\langle(\partial r/\partial t)^2\rangle\approx(w/t)^2$, as in Sec. IV. In terms of Fourier transform, one easily finds, by Eq. (A8),

$$\tilde{K}_{vv}(q)=\lambda^2\left(\frac{w}{t}\right)^2\tilde{f}(q\lambda). \tag{A9}$$

To proceed further, we consider the viscous friction kernels $\gamma(r)$ whose Fourier transform has a power law form

$$\tilde{\gamma}(q)\sim|q|^\alpha, \tag{A10}$$

where α is a positive exponent. Of physical interest are the cases (i) Rouse dynamics, for which $\alpha=0$ and $\gamma(r)\sim\delta_{r,0}$, and (ii) Zimm dynamics, for which $\alpha=1$, see Refs. [28,29]. By using Eqs. (A7) and (A9) with $\tilde{\gamma}(q)$ as in Eq. (A10), it is straightforward to show that

$$p_{\rm diss}=\text{const}\times\left(\frac{w}{t}\right)^2\frac{1}{\lambda^\alpha}. \tag{A11}$$

For the buckling dynamics with $w\sim t^\beta$ and $\lambda\sim t^{n_c}$, we find, by Eq. (A11),

$$p_{\rm diss}(t)\sim t^{-2(1-\beta)-n_c\alpha}, \tag{A12}$$

for the relaxation of dissipation power on the right-hand side of Eq. (A4). The left-hand side of Eq. (A4), $(d/dt)(k+u)$, must decay with the same power law as in Eq. (A12). As in Sec. III, we write down the decay of the elastic energy in the form $u\sim t^{-\delta}$. The decay of the kinetic energy goes as $k=(m/2)\langle v^2\rangle=(m/2)\langle(\partial r/\partial t)^2\rangle=(m/2)(w/t)^2\sim t^{-2(1-\beta)}$. Let us assume that $\delta<2(1-\beta)$. Then, at long times,

$$\frac{d}{dt}(k+u)\approx\frac{d}{dt}u\sim t^{-\delta-1}. \tag{A13}$$

By Eqs. (A13), (A12), and (A4), we thus obtain the scaling relation

$$\delta+1=2(1-\beta)+n_c\alpha, \tag{A14}$$

which reduces to Eq. (18) of Sec. IV for the case of the Rouse dynamics ($\alpha=0$). Equation (A14) can be combined with the equations $n_c=\beta$, and $\delta=n_c(2-\nu)$ of Sec. IV [see Eqs. (19) and (15)] to obtain

$$n_c=\beta=\frac{1}{4-\nu-\alpha} \tag{A15}$$

and

$$\delta=\frac{2-\nu}{4-\nu-\alpha}. \tag{A16}$$

For the case $\alpha=0$, the exponents in Eqs. (A15) and (A16) reduce to the scaling exponents for the Rouse dynamics we found in Sec. IV [see Eqs. (20)–(22)]. For $\alpha=1$, the exponents in Eqs. (A15) and (A16) reduce to the Zimm dynamics exponents anticipated in Eqs. (23)–(25) of Sec. IV. For both of these values of α, the above presumed inequality $\delta<2(1-\beta)$ (i.e., $u\gg k$ at long times) is satisfied.

[1] Y. Kantor, M. Kardar, and D. R. Nelson, Phys. Rev. Lett. **57**, 791 (1986); Phys. Rev. A **35**, 3056 (1987).

[2] F. F. Abraham, W. E. Rudge, and M. Plischke, Phys. Rev. Lett. **62**, 1757 (1989).

[3] G. S. Grest and M. Murat, J. Phys. (France) **51**, 1415 (1990).

[4] G. S. Grest and I. B. Petsche, Phys. Rev. E **50**, 1737 (1994).

[5] D. M. Kroll and G. Gompper, J. Phys. I **3**, 1131 (1993).

[6] T. Hwa, E. Kokufuta, and T. Tanaka, Phys. Rev. A **44**, 2235 (1991).

[7] M. S. Spector, E. Naranjo, S. Chiruvolu, and J. A. Zasadzinski, Phys. Rev. Lett. **73**, 2867 (1994).

[8] J. A. Aronowitz and T. C. Lubensky, Europhys. Lett. **4**, 395 (1987).

[9] D. R. Nelson and L. Peliti, J. Phys. (France) **48**, 1085 (1987); J. A. Aronowitz, L. Golubovic, and T. C. Lubensky, *ibid.* **50**, 609 (1989).

[10] M. Kardar and D. R. Nelson, Phys. Rev. Lett. **58**, 1289 (1987); F. David and K. J. Wiese, *ibid.* **76**, 4564 (1996).

[11] D. Moldovan and L. Golubovic, Phys. Rev. Lett. **82**, 2884 (1999).

[12] L. D. Landau and E. M. Lifshitz, *Theory of Elasticity* (Pergamon, New York, 1986); A. E. Love, *A Treatise on the Mathematical Theory of Elasticity* (Dover, New York, 1994), Chap. 2.
[13] P. Stutenkemper and R. Brasche, in *Proceedings of the Seventh International Conference on Experimental Safety Vehicles, Paris, 1979* (U.S. Department of Transportation, Washington, D.C., 1980).
[14] E. Sackmann, P. Eggl, C. Fahn, H. Ringsdorf, and M. Schollmeier, J. Phys. Chem. **89**, 1198 (1985).
[15] R. R. Chianelli, E. B. Prestige, T. A. Pecoraro, and J. P. DeNeufville, Science **203**, 1105 (1979).
[16] C. F. Schmidt, K. Svoboda, N. Lei, I. B. Petche, L. E. Berman, C. R. Safinya, and G. S. Grest, Science **259**, 952 (1993).
[17] L. Bordieu, J. Daillant, D. Chatenay, A. Braslau, and D. Colson, Phys. Rev. Lett. **72**, 1502 (1994); A. Saint-Jalmes and F. Gallet, Eur. Phys. J. B **2**, 498 (1998).
[18] For buckling induced by internal strains, see, for example, special issue on heteroepitaxy and strain [MRS Bull. **21** (4), (1996)]. For thermally induced buckling, see A. M. Huntz, Mater. Sci. Eng., A **201**, 211 (1995).
[19] L. Golubovic, D. Moldovan, and A. Peredera, Phys. Rev. Lett. **81**, 3387 (1998).
[20] K. Binder, Rep. Prog. Phys. **50**, 783 (1987).
[21] H. Furukawa, Adv. Phys. **34**, 703 (1985).
[22] A. J. Bray, Adv. Phys. **43**, 357 (1994).
[23] H.-J. Ernst, F. Fabre, R. Folkerts, and J. Lapujoulade, Phys. Rev. Lett. **72**, 112 (1994); M. D. Johnson, C. Orme, A. W. Hunt, D. Graff, J. Sudijono, L. M. Sander, and B. G. Orr, *ibid.* **72**, 116 (1994); J. Amar and F. Family, Phys. Rev. B **54**, 14 742 (1996).
[24] L. Golubovic and R. P. U. Karunasiri, Phys. Rev. Lett. **66**, 3156 (1991).
[25] L. Golubovic, Phys. Rev. Lett. **87**, 90 (1997).
[26] A. E. Lobkovsky, S. Gentges, H. Li, D. Morse, and T. A. Witten, Science **270**, 1482 (1995); A. E. Lobkovsky, Phys. Rev. E **53**, 3750 (1996).
[27] E. M. Kramer and T. Witten, Phys. Rev. Lett. **78**, 1303 (1997).
[28] For Zimm effects, see, e.g., E. Frey and D. R. Nelson, J. Phys. I **1**, 1715 (1991), and references therein.
[29] For clarity we note that, for $m=0$, Eq. (A1) implies $\tilde{v}(q,t)=\partial\tilde{r}(q,t)/\partial t=[1/\gamma(q)]\tilde{F}(q)$, where $\tilde{F}(q)$ is the Fourier transform of the elastic force $F(x)=-\partial U/\partial r(x)$. For a free membrane relaxing to the flat configuration $\tilde{F}_T(q,t)\cong-\kappa q^4\tilde{r}_T(q,t)$; thus $\tilde{r}_T(q,t)\sim\exp[-\omega(q)t]$, with $\omega(q)=\kappa q^4/\tilde{\gamma}(q)$. For the Rouse dynamics $\tilde{\gamma}(q)$ is finite for $q\to 0$ and long wavelength membrane undulations r_T relax with $\omega(q)\sim q^4$. For the Zimm dynamics $\gamma(q)\sim|q|$ for small q, and long wavelength undulations of the membrane relax with $\omega(q)\sim q^3$.
[30] See Ref. [12], Chap. 5.